Available online at www.sciencedirect.com

ScienceDirect

Ceramics International 40 (2014) 779–790

CERAMICS INTERNATIONAL

www.elsevier.com/locate/ceramint

Wear and friction behavior of self-lubricating alumina–zirconia–fluoride composites fabricated by the PECS technique

Seung-Ho Kim[a,*], Soo Wohn Lee[b]

[a]Department of Electronics Engineering, Dankook University, 119 Dandae-ro, Dongnam-gu, Cheonan-si, Chungnam 330714, South Korea

[b]Department of Environment Engineering, Sun Moon University, 100 Galsan-ri, Tangjeong-Myeon, Asan, Chungnam 336708, South Korea

Received 10 May 2013; received in revised form 19 June 2013; accepted 19 June 2013
Available online 1 July 2013

Abstract

This study examined the wear and friction behavior of pulse electric current sintered Al_2O_3–ZrO_2 composites containing such fluorides as CaF_2 and BaF_2. The dry sliding wear and friction properties against a commercial alumina bearing ball were investigated using a reciprocal ball-on-plate tribometer. The coefficient of friction of the fluoride-containing Al_2O_3–ZrO_2 composites decreased by approximately 10–20% compared with that of the matrix composite. The wear rate of the fluoride-containing Al_2O_3–ZrO_2 composites was determined to be lower than that of the matrix composite. The following wear rates were observed herein: 0.53×10^{-6} $mm^3/m\,N$ (CaF_2 and low weight fraction of BaF_2), 11.41–45.05×10^{-6} $mm^3/m\,N$ (high weight fraction of BaF_2), and 168.17×10^{-6} $mm^3/m\,N$ (matrix composite). Furthermore, different friction coefficients were observed for the reciprocal sliding test compared with the scratch test due to a difference in the fracture behavior. Because the scratch test employed unidirectional motion, it did not involve fracture behavior due to fatigue or repeated contact.

Keywords: C. Friction; Wear; Self-lubricating; Fluorides; PECS

1. Introduction

Ceramics are relatively hard and brittle materials that exhibit superior resistance to high temperatures and severe environments compared with metals or polymers [1]. In particular, alumina (Al_2O_3) has excellent properties, such as a high melting point, excellent wear resistance and chemical stability. At the same time, this material exhibits lower fracture toughness than other ceramics. Recently, researchers have reported that fracture toughness can be improved by the addition of second phase particles, such as platelets, whiskers, and fibers [2–4]. The fracture toughness and flexural strength can also be enhanced by dispersing nanometer-sized secondary phase materials [5]. The use of tetragonal ZrO_2 (t-ZrO_2) has been shown to improve the mechanical properties of Al_2O_3 ceramics, thereby producing a ceramic known as zirconia toughened alumina (ZTA) [6]. The toughening mechanism of ZTA is based on the stress-induced martensitic transformation and microcrack toughening. The fracture toughness and flexural strength of ZTA are 7 MPa $m^{1/2}$ and 910 MPa, respectively [7].

Ceramics are notably important materials for high-temperature applications in the automotive, aerospace and space shuttle industries. In vehicles, considerable energy is lost due to friction during driving, which accounts for approximately 10% of the energy loss. This problem can be mitigated by friction control and lubrication, as well as increased durability and reliability. In general, friction can be reduced using lubricants, such as oils, greases, gases and solid materials. Because these lubricants are unable to operate at elevated temperatures [8], solid lubricants are better suited for

*Corresponding author. Tel.: +82 41 5503551; fax: +82 41 5503589.
E-mail address: shkim15@dankook.ac.kr (S.-H. Kim).

0272-8842/$ - see front matter © 2013 Elsevier Ltd and Techna Group S.r.l. All rights reserved.
http://dx.doi.org/10.1016/j.ceramint.2013.06.068

high-temperature applications. Solid lubricants, such as CaF_2, BaF_2, $BaCr_2O_4$, $BaCrO_4$, MoS_2, WS_2, h-BN, and graphite, exhibit a lower friction coefficient at high temperatures (773–873 K) than at lower temperatures [9–18]. In general, solid lubricants transition from a brittle state to a plastic state at high temperatures. In particular, the lubricating properties of CaF_2 can be observed above 773 K because this material exists at a slip plane, such as the compacting Ca atomic plane [11].

Tribological behaviors of high temperature components have been raised as an important issue in the application of advanced materials although the following parameters such as microstructure, mechanical properties, and chemical properties have been considered to define the characteristic properties of the mechanical components [19–22]. Microstructures of the material can be optimized by different sintering techniques (conventional sintering techniques such as hot pressing and hot isostatic pressing (HIP), and rapid sintering techniques such as microwave and pulse electric sintering (PECS)) and sintering parameters (such as temperature, pressure, dwell time and heating rates) [23–25]. Especially, PECS technique is a hot pressing system utilizing uniaxial force and a ON–OFF DC pulse energizing under atmospheric pressure to perform high speed consolidation of the powder. The mechanism of PECS is based on high temperature spark plasma momentarily generated in the gaps between neighboring particles [23]. Advantages of PECS techniques compared with conventional sintering techniques are fast sintering process, inhibit grain growth (allowing nanosized grains of the starting powder), and better purification and activation of the particle surfaces [23]. Also, PECS technique has been used to fabricate various materials including metals and alloys, compounds, ceramics, composites, amorphous and nanomaterials [26].

In this paper, the tribological properties of self-lubricating Al_2O_3–ZrO_2 composites containing such fluorides as CaF_2 and BaF_2 were investigated. The composites were fabricated using a PECS technique, and the tribological behavior was evaluated under dry sliding wear and friction conditions.

2. Experimental procedures

2.1. Preparation of powders

Aluminum oxide (α-Al_2O_3, AKP53, Sumitomo Chemical Ltd. Co., Japan), 3 mol% yttrium oxide stabilized zirconium oxide (ZrO_2, TZ-3Y-E, Tosoh Corporation, Japan), calcium fluoride (CaF_2, High Purity Chemicals, Japan), and barium fluoride (BaF_2, High Purity Chemicals, Japan) were used as the starting materials. The ZrO_2 and fluoride contents were set to 15 wt% and 3 wt%, respectively. The powders were ball milled in ethanol for 24 h using a polyethylene pot. The slurry was dried using a vacuum rotary evaporator at 353 K for 2 h and was further dried in an oven at 353 K for 24 h.

2.2. Preparation of test samples

The self-lubricating composites were fabricated by the PECS technique. The sintering conditions were 1573 K and 30 MPa for 5 min under vacuum. The ramp rate was 100 K/min to 1523 K and, subsequently, 25 K/min to 1573 K.

2.3. Density, hardness and fracture toughness tests

The bulk density of the sintered specimens was measured using the Archimedes method. The hardness and fracture toughness of these composites were measured by the Vickers hardness and indentation methods, respectively.

2.4. Wear and friction tests

The wear and friction properties of the composites were evaluated using a reciprocal ball-on-plate tribometer (TE77, Plint and Paterners Ltd., UK). The surface roughness (Ra) of the wear test specimens was below 0.02 μm. A commercial alumina bearing ball (12.7 mm in diameter, Nikkato Corp., Japan) was employed in the wear and friction tests. The experimental conditions included 10 N of applied load, 68 mm/sec of sliding speed for 1 h of sliding time at room temperature without any lubrication. The wear volume was measured by a profilometer (Surfcom 1500SD2, Accretech, Tokyo Seimitsu Co. Ltd., Japan), which tracked 4 points of wear perpendicular to the sliding direction. A planimeter (Super Planix α, Tamaya Technics Inc., Japan) was used to calculate the wear area. The wear rate was calculated using the following equation [8]:

$$\text{wear rate} = V/Pl,$$

where V is wear volume of the specimen, P is the normal load, and l is the total sliding distance. The morphology of fractured and worn surfaces of the composites was examined by scanning electron microscopy (SEM).

3. Results and discussion

3.1. Microstructural analysis

Fig. 1 provides the X-ray diffraction patterns of Al_2O_3–ZrO_2 composites prepared with CaF_2 and BaF_2. The X-ray diffraction patterns of the Al_2O_3–ZrO_2 composites were different due to the presence of CaF_2 and BaF_2. In the case of the CaF_2 containing composites, no additional products were observed. The ZrO_2 phase exhibited a complete transition from the monoclinic to the tetragonal phase. In contrast, the monoclinic ZrO_2 phase was observed for composites containing BaF_2. As the BaF_2 content increased, the degree of monoclinic ZrO_2 phase also increased. The presence of BaF_2 in the Al_2O_3–ZrO_2 composite inhibited the phase transformation from the monoclinic to the tetragonal phase of ZrO_2.

Fig. 2 shows the SEM micrographs of Al_2O_3–ZrO_2 composites in the presence and absence of different solid lubricants, such as CaF_2 and BaF_2. Fig. 2(a) demonstrates that the grain size of Al_2O_3 in the Al_2O_3–ZrO_2 composite was below 600 nm in the absence of a solid lubricant. However, the grain size of Al_2O_3 in the presence of the lubricant was greater than in the absence of the lubricant, as shown in Fig. 2(b) and (c).

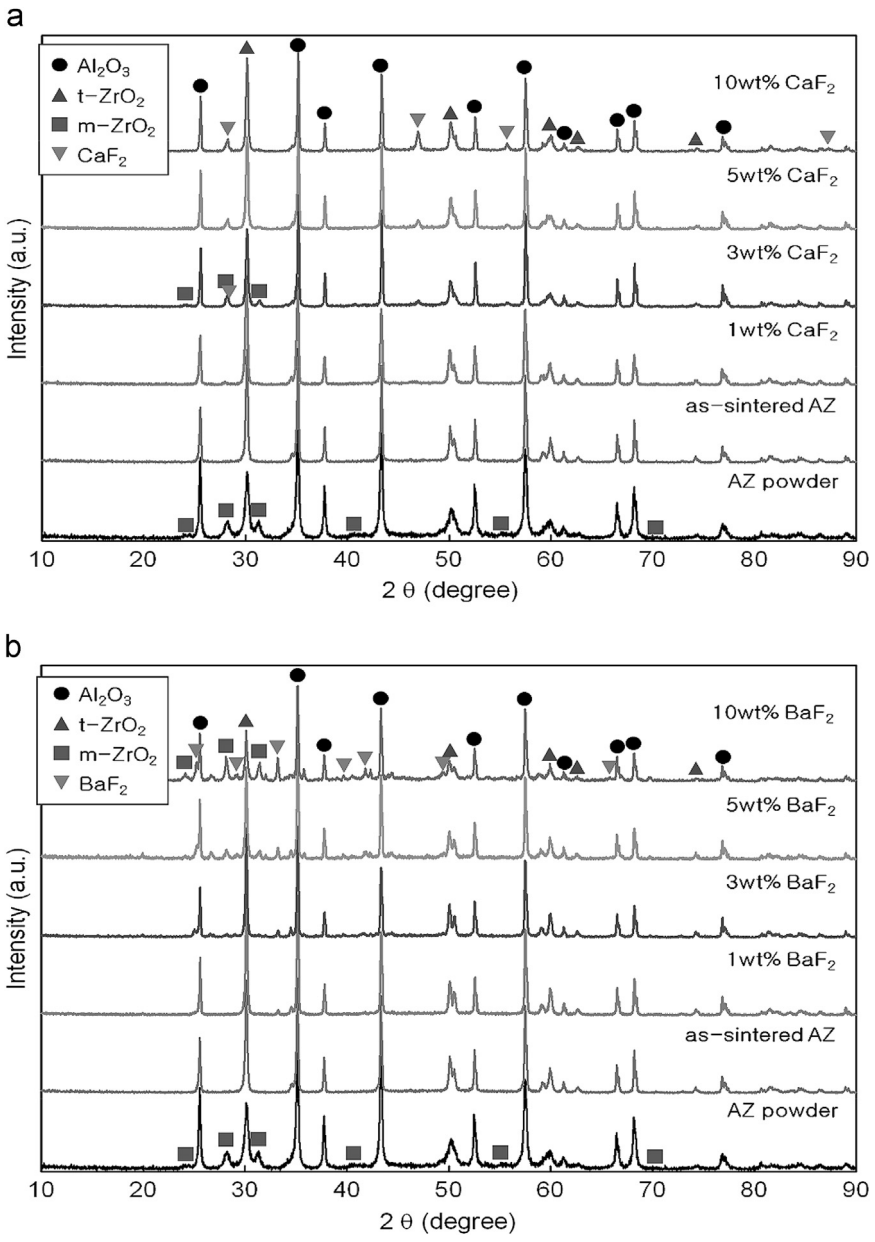

Fig. 1. X-ray diffraction patterns of Al_2O_3-15 wt% ZrO_2 containing different solid lubricants: (a) CaF_2 and (b) BaF_2.

The grain size of Al_2O_3 in the CaF_2 containing Al_2O_3–ZrO_2 composite was larger than that of its BaF_2 counterpart with a size of more than 1 μm and a coarsened appearance. Whereas the grain growth of Al_2O_3 in the Al_2O_3–ZrO_2 composite was affected by the presence of CaF_2, BaF_2 was observed as several micrometer plate-shaped particles in the Al_2O_3–ZrO_2 composite. The microstructure of Al_2O_3–ZrO_2 composites in the absence and presence of solid lubricants exhibited an effect on the mechanical properties, as well as the wear and friction behavior of the materials.

3.2. Mechanical properties

The relative density of Al_2O_3–ZrO_2 composites containing BaF_2 was related to the presence of the monoclinic ZrO_2 phase (Fig. 3(a)). An increase in the amount of additives caused a decrease in the hardness of the Al_2O_3–ZrO_2 composite (Fig. 3(b)) because of the lower hardness values of CaF_2 and BaF_2 relative to the matrix composite. The grain growth of Al_2O_3 in the CaF_2 and BaF_2 containing Al_2O_3–ZrO_2 composites is shown in Fig. 2(a)–(c). The low hardness of the matrix composite is attributed to the low density of the solid lubricants. In these samples, the ratio of CaF_2 (or BaF_2)/Al_2O_3 increased from 0.0119 (1 wt%) to 0.1333 (10 wt%). Increasing the amount of solid lubricant led to a decrease in the hardness of the Al_2O_3–ZrO_2 composites. In contrast, the fracture toughness of the composites exhibited different trends with respect to the additive content (Fig. 3(c)). The fracture toughness of the CaF_2 containing composite decreased with increasing CaF_2 content, whereas that of the BaF_2 containing

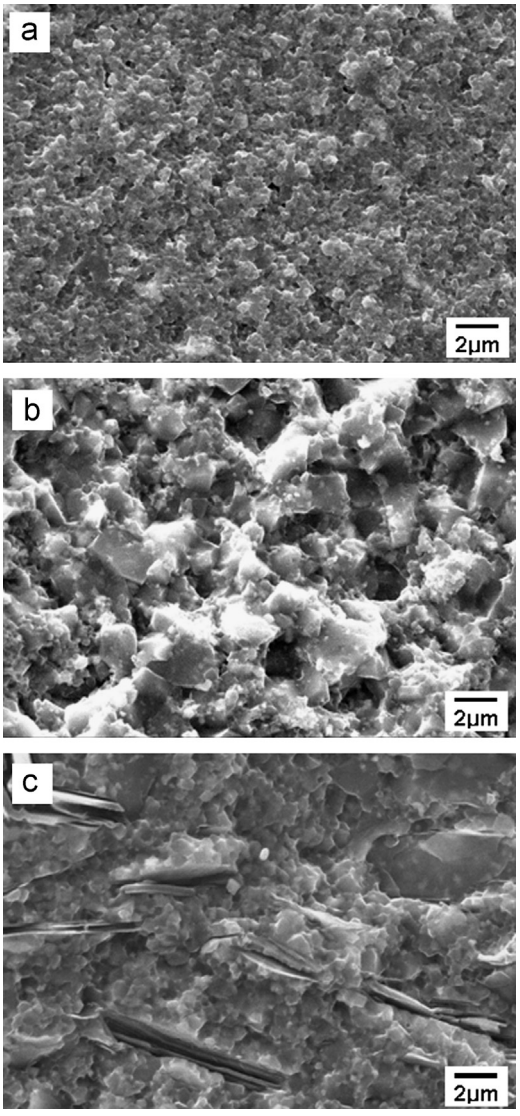

Fig. 2. SEM micrographs of Al_2O_3-15 wt% ZrO_2 composites containing different solid lubricants: (a) absence of lubricants (matrix), (b) CaF_2, and (c) BaF_2.

composite increased with increasing BaF_2 content. The increase in the fracture toughness of the latter lubricant is related to the dispersion of the plate-shaped BaF_2 domains and the large grain size of the Al_2O_3–ZrO_2. Similarly, the increased toughness caused by the presence of BaF_2 was due to crack deflection and bridging along the plate-shaped BaF_2 domains. The fracture toughness of the Al_2O_3–ZrO_2 composites was closely related to the shape of the lubricants in the composite.

3.3. Wear and friction behavior

The coefficient of friction and wear rate of the Al_2O_3–ZrO_2 composites are shown in Figs. 4 and 5. The coefficient of friction of Al_2O_3–ZrO_2 composite containing solid lubricants was lower than that of the matrix Al_2O_3–ZrO_2 composite. The coefficient of friction of the latter material decreased from 0.5 to 0.35 when the sliding time was increased. At the same time, the friction coefficient of the CaF_2 containing Al_2O_3–ZrO_2 composites remained constant in the range of 0.3–0.5, except for the specimen containing 3 wt% CaF_2, which was approximately 0.25. In contrast, the coefficient of friction of the BaF_2 containing Al_2O_3–ZrO_2 composite varied as a function of sliding time. As the sliding time increased, the coefficient of friction exhibited two different regimes with varying BaF_2 content. The coefficient of friction of composites containing a low fraction of BaF_2 (1 wt% and 3 wt% BaF_2) increased slightly, whereas those containing a high fraction of BaF_2 (5 wt% and 10 wt% BaF_2) decreased to approximately 0.1. The friction coefficient of composites containing solid lubricants was similar to that of the matrix composite as a function of sliding time.

Wear debris observed in solid lubricant containing Al_2O_3–ZrO_2 composites during the wear and frictions tests were not caused by the presence of lubricants but instead were a result of a cushion created by a decrease in the shear stress. Therefore, the coefficient of friction of the lubricant containing Al_2O_3–ZrO_2 composites approached that of the matrix composite.

Fig. 5 shows the wear rates of the Al_2O_3–ZrO_2 composites as a function of solid lubricants content. The wear rate of the solid lubricant containing Al_2O_3–ZrO_2 composites was lower than that of the matrix Al_2O_3–ZrO_2 composite. As the amount of CaF_2 increased, the wear rate of the Al_2O_3–ZrO_2 composite remained constant between 0.25 and 0.40×10^{-6} mm^3/m N, which was several times higher than that of other composites. In contrast, the wear rate of the BaF_2 containing Al_2O_3–ZrO_2 composite increased with increasing BaF_2 content from 0.36 to 45.05×10^{-6} mm^3/m N. In particular, the wear rate of the composites increased dramatically above 5 wt% BaF_2. Furthermore, the wear rate of the BaF_2 containing Al_2O_3–ZrO_2 composite was closely related to the initial friction coefficient. The initial friction coefficient of the low fraction composites (1 wt% and 3 wt% BaF_2) was approximately 0.33–0.34, whereas that of the high fraction composites (5 wt% and 10 wt% BaF_2) composites was approximately 0.47–0.51. Conversely, the steady-state friction coefficient of the low and high fraction composites was similar in the range of 0.33–0.38. In the case of BaF_2 containing composites, the wear rates were closely related to the friction coefficient behavior of the material. The initial friction coefficient was affected by the presence of fracture or microcracks. The high wear rate of the Al_2O_3–ZrO_2 composite containing 10 wt% BaF_2 was caused by the long dwell times of the high initial friction coefficient. In contrast, the wear rate of the Al_2O_3–ZrO_2 composite containing 5 wt% BaF_2 was lower than that of composite containing 10 wt% BaF_2. The friction coefficient of the Al_2O_3–ZrO_2 composite containing 5 wt% BaF_2 decreased gradually with increasing sliding time.

The tribological behavior and the wear rate of the solid lubricant containing Al_2O_3–ZrO_2 composites can be explained by the SEM micrographs of the worn surfaces shown in Figs. 6–8. Fig. 6 shows the worn surface of the matrix Al_2O_3–ZrO_2 composite, revealing two different types of surface morphologies, including rough and smooth surfaces. The region with a rough surface exhibited signs of fracture and

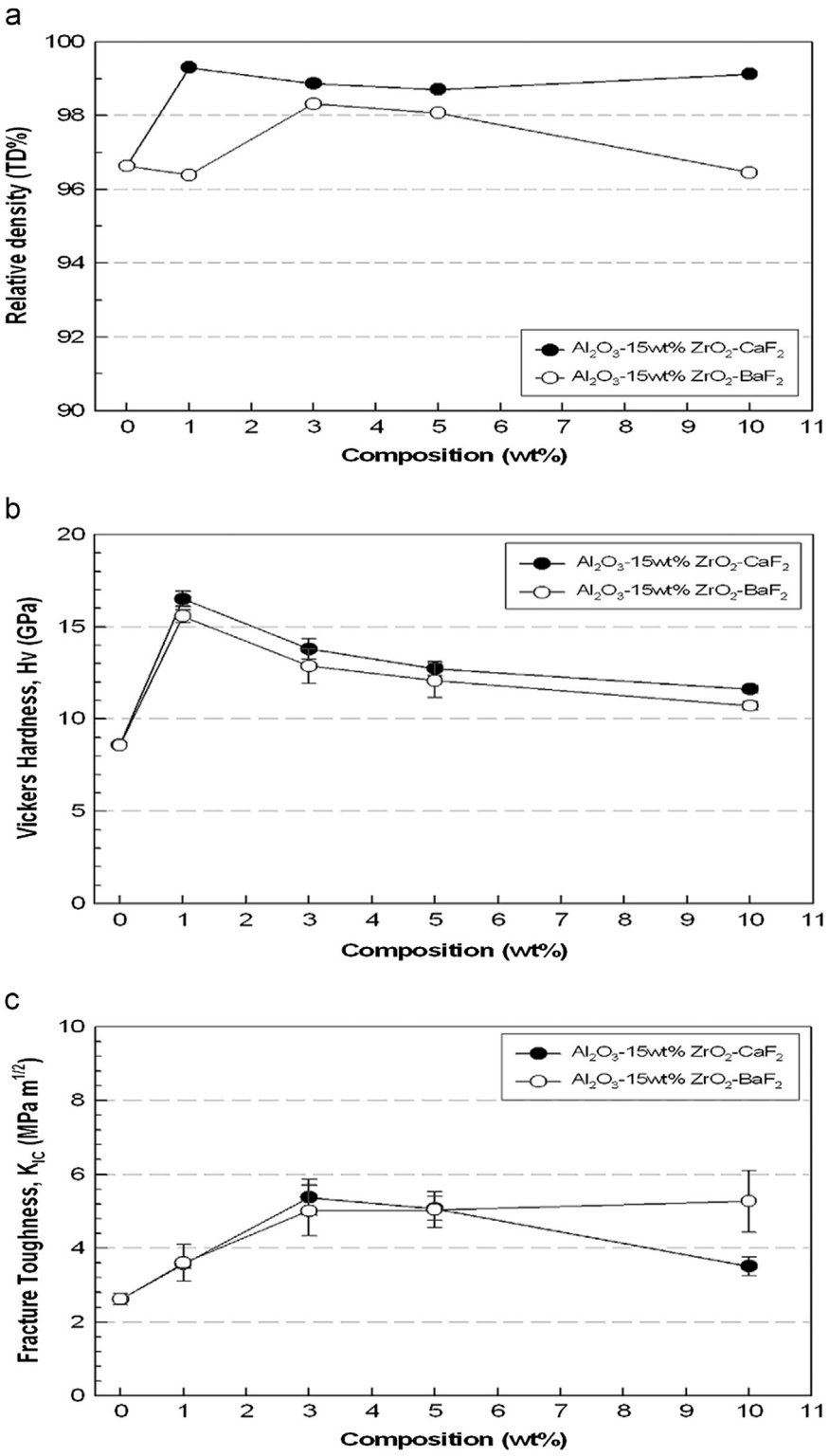

Fig. 3. Mechanical properties of Al_2O_3-15 wt% ZrO_2 composites prepared with different solid lubricants: (a) the relative density, (b) hardness and (c) fracture toughness.

chipping due to the presence of microcracks. In contrast, the smooth surface of the matrix Al_2O_3–ZrO_2 composite featured a wear debris film caused by shear stresses. In addition, microcracks were also observed in the wear debris of the film. The friction coefficient of the Al_2O_3–ZrO_2 composites was affected by the repetitive formation and fracture of the wear debris films during the wear and friction tests. The coefficient of friction of the Al_2O_3–ZrO_2 composites increased due to the rough nature of the worn surface and the presence of large pieces of wear debris.

The wear and friction behavior of Al_2O_3–ZrO_2 composites containing solid lubricants was affected by the characteristics

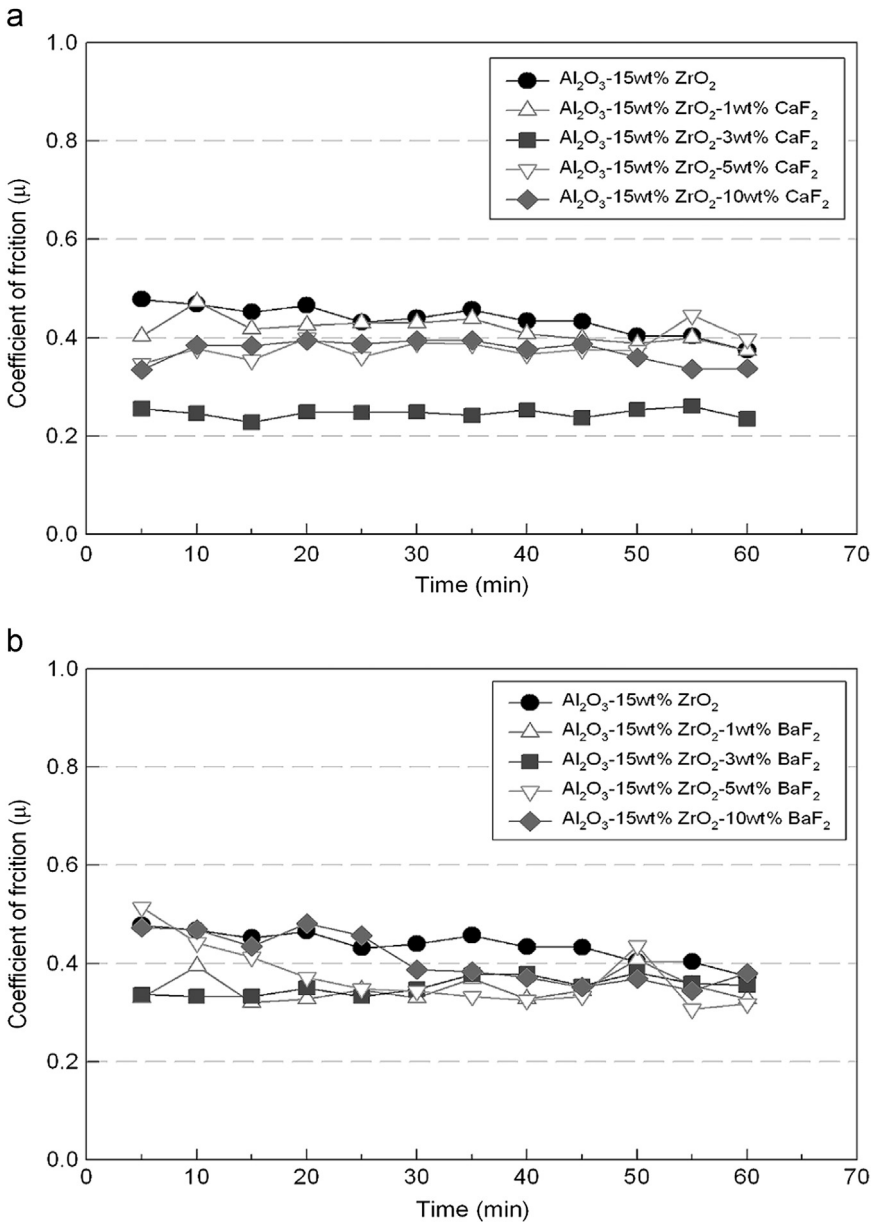

Fig. 4. The coefficient of friction of Al_2O_3-15 wt% ZrO_2 composites containing different solid lubricants: (a) CaF_2 and (b) BaF_2.

of the solid lubricants. The wear and friction behavior of the Al_2O_3–ZrO_2 composites containing solid lubricants, such as CaF_2 and BaF_2, is compared in Figs. 7 and 8. The CaF_2 containing Al_2O_3–ZrO_2 composite exhibited a smooth-worn surface, which did not change as a function of CaF_2 content.

Fine wear debris can be observed in the worn surface of the composite, as well as the wear debris-filled pores, as shown in the high magnitude SEM micrographs. The smooth worn surface of the CaF_2 containing Al_2O_3–ZrO_2 composite led to a decrease in the friction coefficient and wear rate. In contrast, the surface roughness of the BaF_2 containing Al_2O_3–ZrO_2 composite increased with increasing BaF_2 content, as shown in Fig. 8. As the amount of BaF_2 increased, the number of microcracks on the worn surface also increased. The worn surface of the low weight fraction composites (1 wt% and 3 wt % BaF_2) exhibited similar trends to those of the CaF_2 containing composites, in which fine wear debris were observed on the worn surface. The low wear rates and friction coefficients of the composites containing a low weight fraction of BaF_2 were due to the smooth worn surface. A relatively thick debris film was observed on the worn surface of BaF_2 containing Al_2O_3–ZrO_2 composites. However, the wear rate of the Al_2O_3–ZrO_2 composites containing BaF_2 increased with increasing BaF_2 content because the wear debris could be easily generated and removed over the course of the wear and friction test. Although a thick wear debris film was generated, the increasing wear rate of the BaF_2 containing Al_2O_3–ZrO_2 composites was caused by the soft and weak nature of the film. The size of the wear debris of this composite was smaller than that of the matrix composite, as shown in Figs. 6 and 8.

The low friction coefficient and wear rate were caused by the presence of fine wear debris particles. Over the course of

the wear and friction test, the friction coefficient increased due to the presence of large wear debris between the composites and the ball. The initial phase of the wear and friction test generated large wear debris particles, which were then broken down into smaller pieces between the composite and the ball during the wear and friction test. The change in the friction coefficient of the BaF_2 containing Al_2O_3–ZrO_2 composites suggests that the fine-sized wear debris filled regions of pores, pulling on the grains or chipping away at the worn surfaces of the composite. The generation of large wear debris particles during the sliding process was inhibited due to the presence of a wear debris film. In this manner, the coefficient of friction of the BaF_2 containing Al_2O_3–ZrO_2 composites decreased with increasing sliding time.

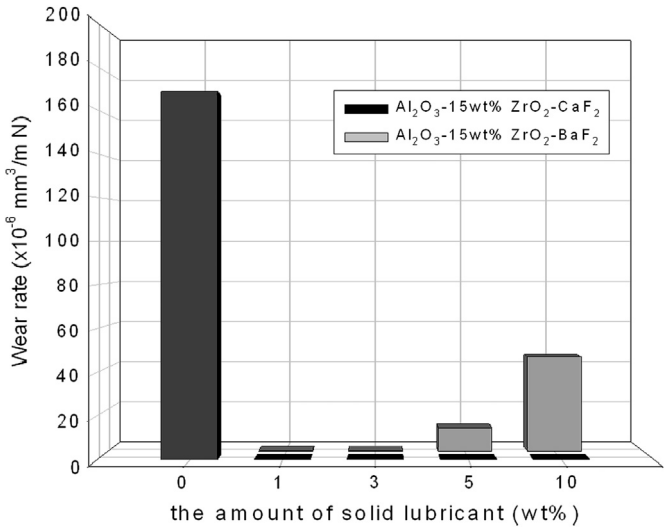

Fig. 5. The wear rates of Al_2O_3-15 wt% ZrO_2 composites containing different solid lubricants.

3.4. Friction behavior observed using the scratch test

Figs. 9–11 provide the scratch test results of the Al_2O_3–ZrO_2 composites prepared using different solid lubricants. In general, the results obtained using the scratch test were different from those of the reciprocal ball-on-plate test. Typically, the coefficient of friction of composites containing solid lubricants is lower than that of the matrix composite, which was also observed in this study with the reciprocal ball-on-plate method. However, the coefficient of friction of the Al_2O_3–ZrO_2 composites containing solid lubricants as determined by the scratch test was actually higher than that of the matrix composite. The friction coefficient of the Al_2O_3–ZrO_2 composite in the absence of the solid lubricant was 0.56 in the initial region and 0.32 in the steady-state region. In contrast, the coefficient of friction of the CaF_2 and BaF_2 containing Al_2O_3–ZrO_2 composite gradually decreased with increasing applied load. In the initial region, the coefficient of friction of the Al_2O_3–ZrO_2 composites containing CaF_2 and BaF_2 was 0.65–0.77 and 0.75–1.0, respectively. Over time, the steady-state value decreased to 0.35–0.45 and 0.35–0.60, respectively. The difference in the behavior of Al_2O_3–ZrO_2 composites containing fluoride solid lubricants was caused by variations in the surface morphologies due to the presence of soft solid lubricants and a weak interface between the matrix and the solid lubricant. When the applied load was above a certain threshold, the solid lubricant at the interface could be easily removed during the sliding process. As shown in Figs. 9–11, the variation in the coefficient of friction at low applied loads

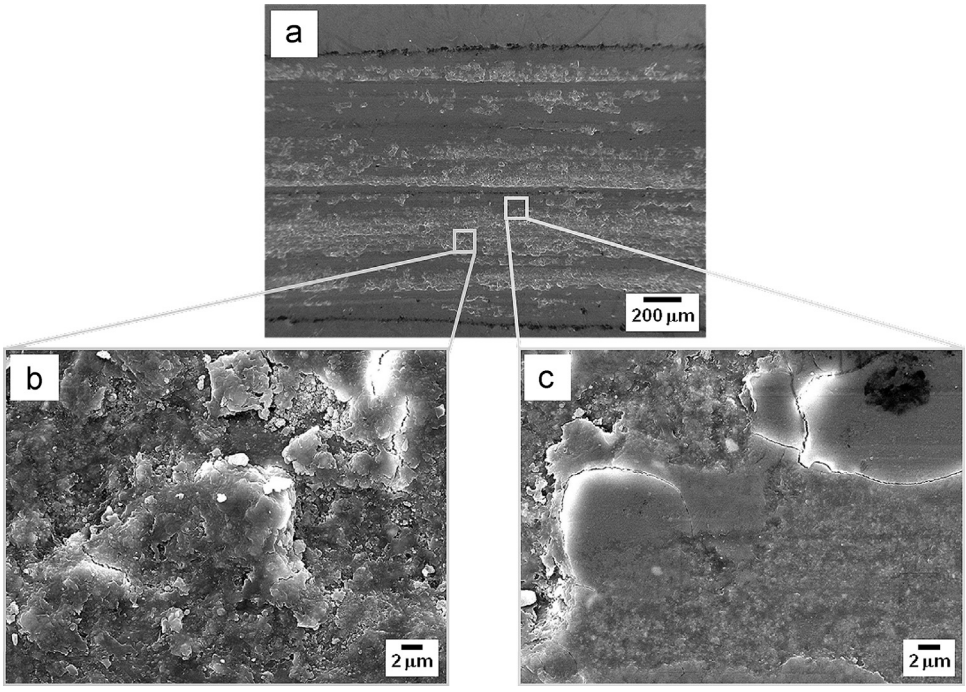

Fig. 6. SEM micrographs of the worn surface of Al_2O_3-15 wt% ZrO_2 composites: (a) obtained at a low magnitude, (b) uncovered wear debris films at a high magnitude, and (c) covered wear debris film at a high magnitude.

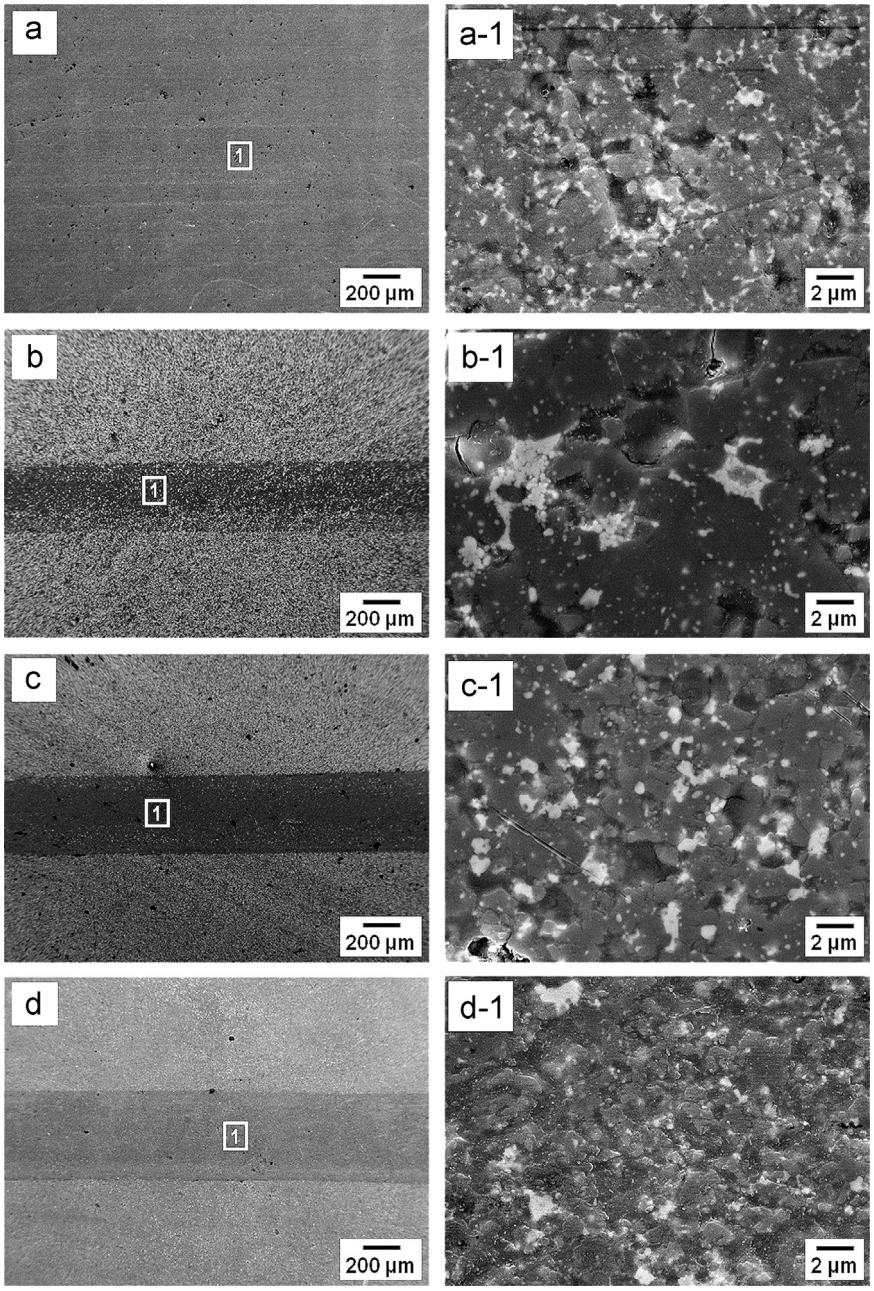

Fig. 7. SEM micrographs of the worn surface of Al_2O_3-15 wt% ZrO_2 composites containing different amounts of CaF_2: (a) 1 wt%, (b) 3 wt%, (c) 5 wt%, and (d) 10 wt%.

(below the threshold) is related to the surface morphology (or roughness) and the weak contact between the diamond stylus and the surface. In contrast, at high applied loads (above the threshold), the coefficient of friction was affected by the surface properties, such as hardness, interfacial strength and microstructure (including the distribution and directionality of the solid lubricant).

Furthermore, the difference in the observed friction coefficients of Al_2O_3–ZrO_2 composites prepared with different solid lubricants was caused by the different measurement techniques, specifically, the degree of repeated contact between the counterpart and the specimen [15], the size of the contact area due to the size of counterpart (a diameter of 12.7 mm for the alumina ball versus a radius of 200 μm for the Rockwell diamond tip), and the nature of the counterpart material (alumina versus diamond). Furthermore, the high initial frictional coefficient of the solid lubricant containing Al_2O_3–ZrO_2 composites during the reciprocal ball-on-plate method and scratch test was caused by the high contact pressure due to the reduced contact area between the counterpart and the specimen. As the applied load increased during the scratch test, the contact pressure decreased due to the increasing contact area between the counterpart and the specimen. Similarly, in the case of the reciprocal ball-on-plate method, when the contact area of the counterpart increased during the sliding process, the contact pressure between the counterpart and the specimen

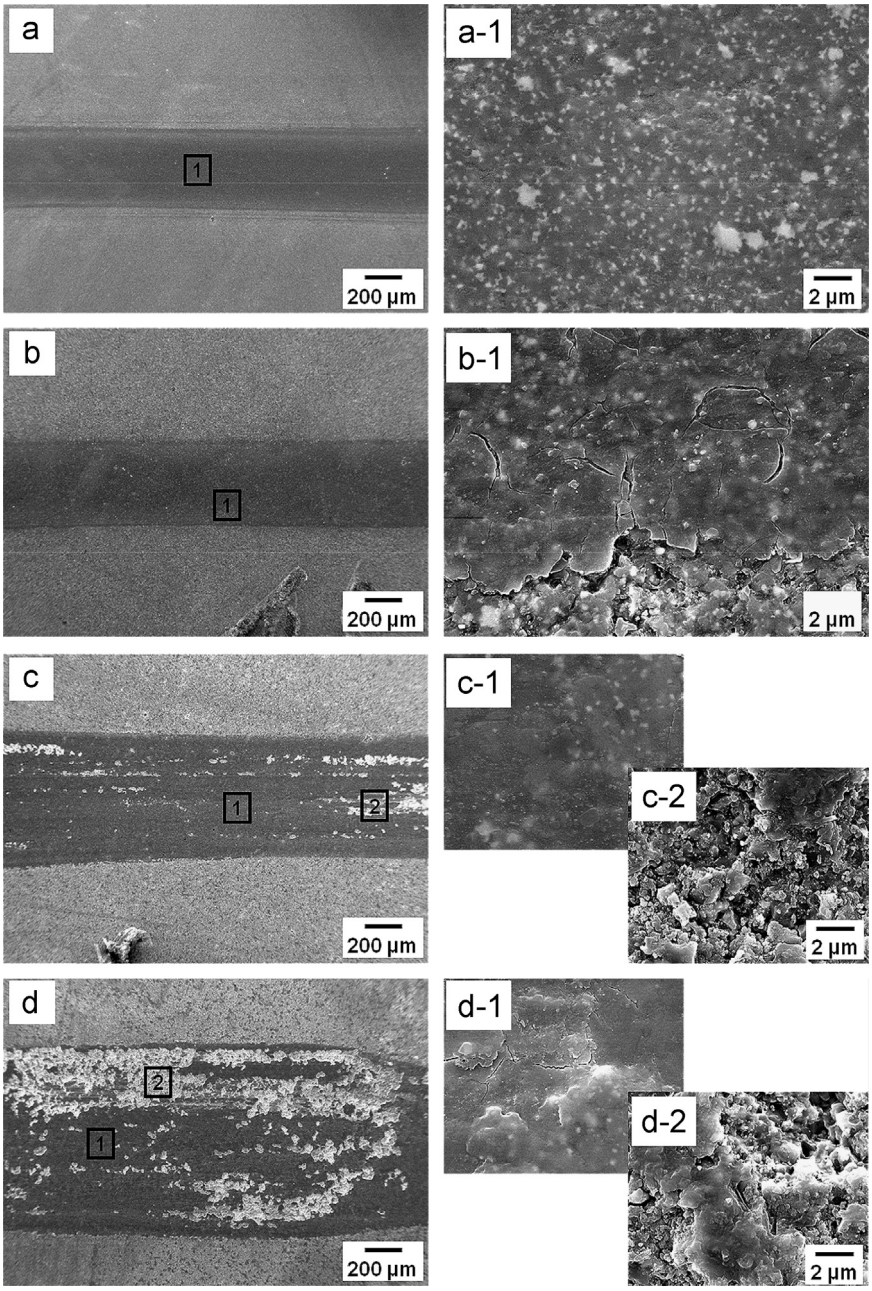

Fig. 8. SEM micrographs of the worn surface of Al_2O_3-15 wt% ZrO_2 composites containing different amounts of BaF_2: (a) 1 wt%, (b) 3 wt%, (c) 5 wt% and (d) 10 wt%.

decreased. In addition, the fracture behavior caused by the reciprocal ball-on-plate method was entirely different from that of the scratch test. During the reciprocal sliding test, the fracture behavior was accompanied by fatigue due to the repeated contact between the counterpart and the specimen [15]. These reciprocal motions during the wear and friction test broke up the wear debris into much smaller pieces, forming a transfer film on the worn surface, which, in turn, decreased the coefficient of friction during the sliding process. In contrast, because the scratch test was performed using unidirectional motion, the fatigue type fracture behavior was not observed. Finally, the coefficient of friction for the scratch test was affected by the interfacial properties between the counterpart and the specimen, as well as the characteristics of both specimens.

4. Conclusions

The wear and friction behavior of pulse electric current sintered Al_2O_3–ZrO_2 composites containing CaF_2 and BaF_2 lubricants was investigated. Wear and friction tests were performed using a reciprocal ball-on-plate tribometer and a scratch tester to compare the coefficient of friction obtained using the two different techniques. The ZrO_2 phase in the CaF_2 containing Al_2O_3–ZrO_2 composite transitioned from the monoclinic to the tetragonal phase. In contrast, the presence of the

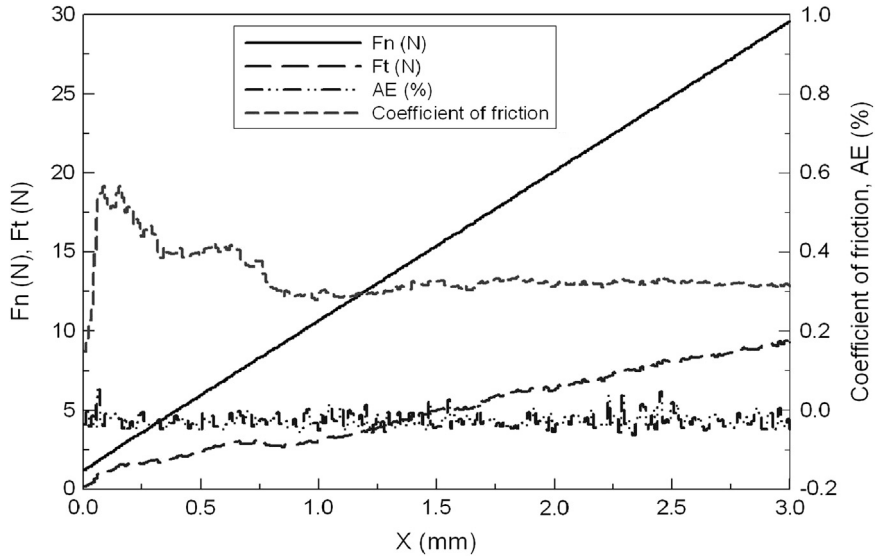

Fig. 9. The scratch test results of Al_2O_3-15 wt% ZrO_2 composites prepared in the absence of a solid lubricant (*X*: scratch length and applied load: 1 to 30 N).

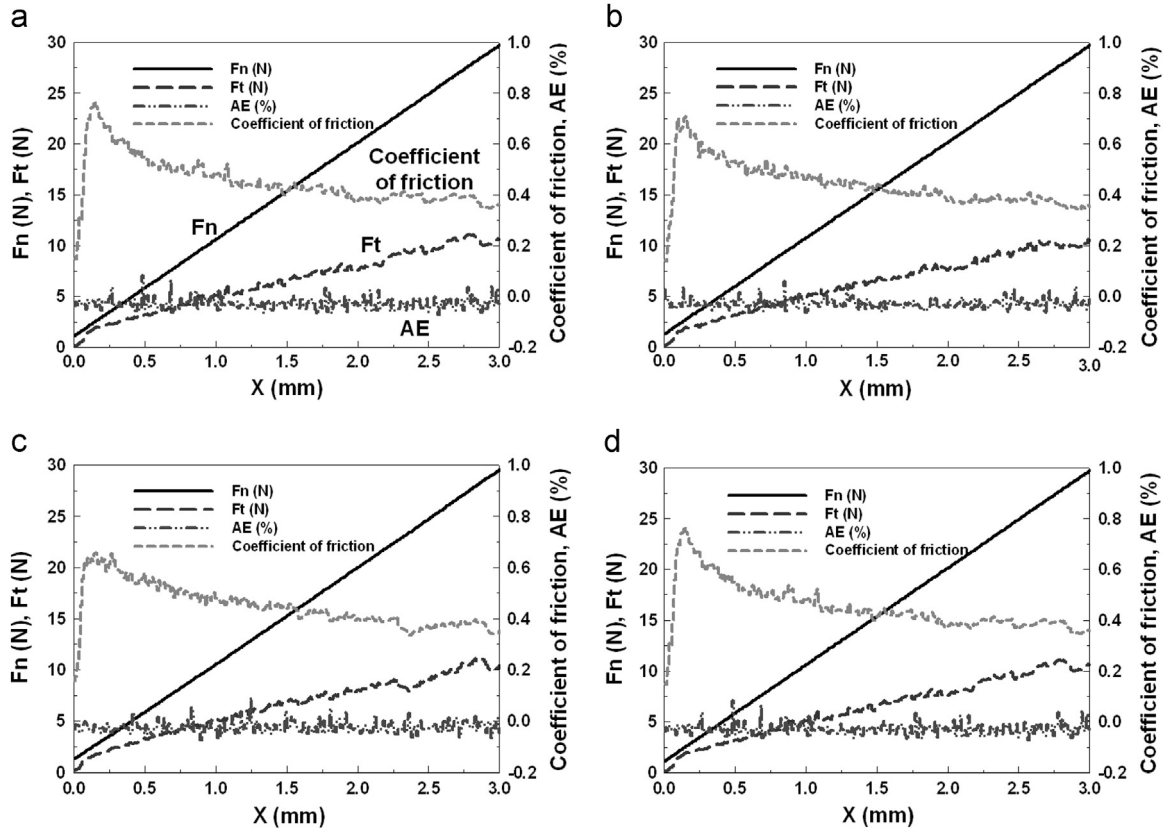

Fig. 10. The scratch test results of Al_2O_3-15 wt% ZrO_2 composites containing different amounts of CaF_2: (a) 1 wt%, (b) 3 wt%, (c) 5 wt%, and (d) 10 wt% (*X*: scratch length and applied load: 1 to 30 N).

monoclinic ZrO_2 phase also increased with increasing BaF_2 content. Indeed, the presence of BaF_2 in the Al_2O_3–ZrO_2 composite was found to inhibit the monoclinic to tetragonal phase change of the ZrO_2. All materials produced in this study exhibited a coefficient of friction in the range of 0.31–0.51 with the exception of the composite containing 3 wt% CaF_2, which exhibited a coefficient between 0.23 and 0.26. The wear rates of the composites were closely related to nature and concentration of the solid lubricants. The wear rates were found to range from less than 0.53×10^{-6} $mm^3/m\,N$ for CaF_2 and low weight fraction of BaF_2, to between 11.41 and 45.05×10^{-6} $mm^3/m\,N$ for the high weight fraction of BaF_2,

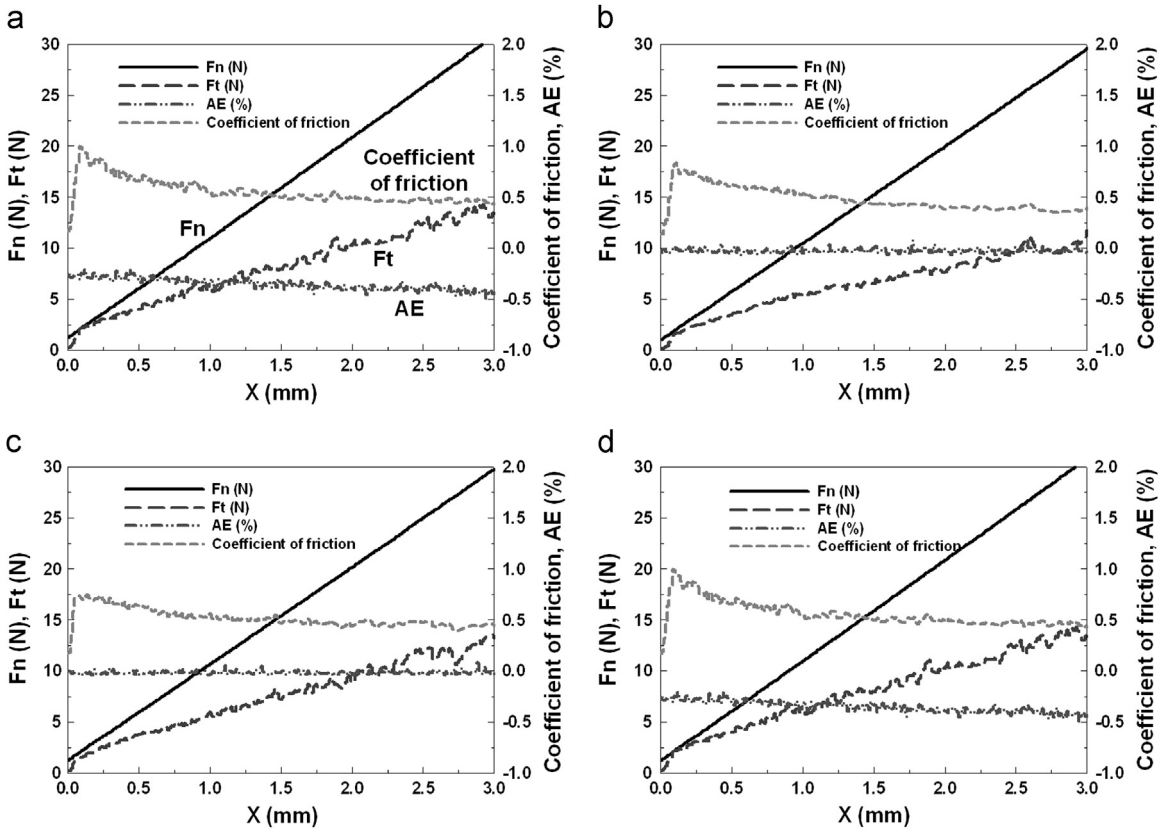

Fig. 11. The scratch test results of Al_2O_3-15 wt% ZrO_2 composites containing different amounts of BaF_2; (a) 1 wt%, (b) 3 wt%, (c) 5 wt%, and (d) 10 wt% (*X*: scratch length and applied load: 1 to 30 N).

to as high as 168.17×10^{-6} $mm^3/m\,N$ for the matrix composite. The worn surfaces of the low wear rate specimens exhibited fine wear debris particles and the presence of a thin transfer film. In contrast, the worn surfaces of high wear rate specimens exhibited large wear debris particles and a thicker, weakened transfer film. Furthermore, the coefficient of friction measured using the scratch test was higher than that of the reciprocal sliding test. In fact, even the matrix composite exhibited a lower friction coefficient than the fluoride containing composites according to the scratch test. The difference in the friction coefficient is due to a difference in the fracture behavior resulting from the two testing methods. Because the scratch test employs unidirectional motion, it did not involve such phenomena as fracture fatigue due to repeated contact. Finally, the coefficient of friction measured by the scratch test is also affected by the interfacial properties between the counterpart and the specimen, as well as the physical characteristics of both specimens.

Acknowledgments

This work was supported by the Korea Foundation for International Cooperation of Science and Technology (KICOS 2008-0143) and the Global Research Laboratory (GRL) program of the National Research Foundation of Korea (NRF) funded by Ministry of Education, Science and Technology (MEST) of Korea (Grant number 2010-00339).

References

[1] L.H. Van Vlack, Elements of Materials Science and Engineering, sixth ed., Addison-Wesley Pub., 1990.
[2] M.M. Schwartz, Composite Materials, Volume 1: Properties, Nondestructive, Testing, and Repair, Prentice-Hall PTR, 1997.
[3] X. Yang, M.N. Rahaman, SiC platelet reinforced Al_2O_3 composites by free sintering of coated powders, Ceramic Engineering and Science Proceeding 15 (1994) 702–709.
[4] C.L. Hu, M.N. Rahaman, SiC-whisker-reinforced Al_2O_3 composites by free sintering of coated powder, Journal of the American Ceramic Society 76 (1993) 2549–2554.
[5] K. Niihara, New design concept of structural ceramics: ceramic nanocomposites, Journal of the Ceramic Society of Japan 99 (1991) 945–952.
[6] A.K. Deb, P. Chatterjee, S.P. Sen Gupta, Synthesis and microstructural characterization of α-Al_2O_3–t-ZrO_2 composite powders prepared by combustion technique, Materials Science and Engineering A 459 (2007) 124–131.
[7] M. Ruhle, N. Claussen, A.H. Heuer, Transformation and microcrack toughening as complementary processes in ZrO_2-toughened Al_2O_3, Journal of the American Ceramic Society 69 (1986) 195–197.
[8] N.K. Myshkin, C.K. Kim, M.I. Petrokovets, Introduction to Tribology, Cheong Moon Gak, 1997.
[9] J.H. Ouyang, S. Sasaki, Effects of different additives on microstructure and high-temperature tribological properties of plasma-sprayed Cr_2O_3 ceramic coatings, Wear 249 (2001) 56–57.
[10] J.H. Ouyang, S. Sasaki, T. Murakami, K. Umeda, The synergistic effects of CaF_2 and Au lubricants on tribological properties of spark-plasma-sintered $ZrO_2(Y_2O_3)$ matrix composites, Materials Science and Engineering A 386 (2004) 234–243.
[11] Z. Liu, T.H.C. Childs, The influence of TiC, CaF_2 and MnS additives on friction and lubrication of sintered high speed steels at elevated temperature, Wear 193 (1996) 31–37.

[12] J.H. Ouyang, S. Sasaki, K. Umeda, Low-pressure plasma-sprayed ZrO_2–CaF_2 composite coating for high temperature tribological applications, Surface and Coatings Technology 137 (2001) 21–30.

[13] J.H. Ouyang, S. Sasaki, T. Murakami, K. Umeda, Spark-plasma-sintered $ZrO_2(Y_2O_3)$–$BaCrO_4$ self-lubricating composites for high temperature tribological applications, Ceramics International 31 (2005) 543–553.

[14] T. Murakami, J.H. Ouyang, S. Sasaki, K. Umeda, Y. Yoneyama, High-temperature tribological properties of Al_2O_3, Ni-20 mass% Cr and NiAl spark-plasma sintered composites containing BaF_2–CaF_2 phase, Wear 259 (2005) 626–633.

[15] S.H. Kim, S.P. Hannula, S.W. Lee, Effects of the sliding conditions on the tribological behavior of atmospheric plasma sprayed Al_2O_3-15 wt% ZrO_2–CaF_2 composite coating, Surface and Coatings Technology 210 (2012) 127–134.

[16] M.E. Cura, S.H. Kim, T. Muukkonen, S. Varjus, A. Vaajoki, O. Söderberg, T. Suhonen, U. Kanerva, S.W. Lee, S.P. Hannula, Microstructure and tribological properties of pulsed electric current sintered alumina–zirconia nanocomposites with different solid lubricants, Ceramics International 39 (2013) 2093–2105.

[17] S.H. Kim, S.H. Cho, S.P. Hannula, S.W. Lee, Effects of different solid lubricants on mechanical and tribological properties of Al_2O_3/ZrO_2 nanocomposites, Materials Science Forum 658 (2010) 404–407.

[18] M.E. Cura, S.H. Kim, S.H. Cho, T. Suhonen, T. Muukkonen, A. Vaajoki, O. Söderberg, U. Kanerva, S.W. Lee, S.P. Hannula, Pulsed electric current sintering of the Al_2O_3-15 wt% ZrO_2 nanocomposites with 3 wt% of different solid lubricants, Materials Science Forum 695 (2011) 473–476.

[19] S.J. Cho, B.J. Hockey, B.R. Lawn, S.J. Bennison, Grain-size and R-curve effects in the abrasive wear of alumina, Journal of the American Ceramic Society 72 (1989) 1249–1252.

[20] Y.N. Liang, S.W. Lee, D.S. Park, Effects of whisker distribution and sintering temperature on friction and wear of Si_3N_4-whisker-reinforced Si_3N_4-composites, Wear (225–229) (1999) 1327–1337.

[21] T.E. Fischer, M.P. Anderson, S. Jahanmir, Influence of fracture toughness on the wear resistance of ytrria-doped zirconium oxide, Journal of the American Ceramic Society 72 (1989) 252–257.

[22] S. Jahanmir, T.E. Fischer, Friction and wear of silicon nitride lubricated by humid air, water, hexadecane and hexadecane +0.5 percent stearic acid, STLE Transactions 31 (1988) 32–34.

[23] D. Tiwari, B. Basu, K. Biswas, Simulation of thermal and electric field evolution during spark plasma sintering, Ceramics International 35 (2009) 699–708.

[24] D.D. Jayaseelan, N. Kondo, D.A. Rani, S. Ueno, T. Ohji, S. Kanzaki, Pulse electric current sintering of Al_2O_3/3 vol% ZrO_2 with constrained grains and high strength, Journal of the American Ceramic Society 85 (2002) 2870–2872.

[25] B. Basu, J.-H. Lee, D.-Y. Kim, Development of nanocrystalline wear-resistant Y-TZP ceramics, Journal of the American Ceramic Society 87 (2004) 1771–1774.

[26] M. Suganuma, Y. Kitagawa, S. Wada, N. Murayama, Pulsed electric current sintering of silicon nitride, Journal of the American Ceramic Society 86 (2003) 387–394.